

Voltage-control of damping constant in magnetic–insulator/topological–insulator bilayers

Takahiro Chiba,¹ Alejandro O. Leon,² and Takashi Komine³

¹*National Institute of Technology, Fukushima College, 30 Nagao, Kamiarakawa, Taira, Iwaki, Fukushima 970-8034, Japan*

²*Departamento de Física, Facultad de Ciencias Universidad Tecnológica Metropolitana, Las Palmeras 3360, Ñuñoa 780-0003, Santiago, Chile*

³*Graduate School of Science and Engineering, Ibaraki University, 4-12-1 Nakanarusawa, Hitachi, Ibaraki 316-8511, Japan*

(Dated: 8 June 2021)

The magnetic damping constant is a critical parameter for magnetization dynamics and the efficiency of memory devices and magnon transport. Therefore, its manipulation by electric fields is crucial in spintronics. Here, we theoretically demonstrate the voltage-control of magnetic damping in ferro- and ferrimagnetic–insulator (FI)/topological–insulator (TI) bilayers. Assuming a capacitor-like setup, we formulate an effective dissipation torque induced by spin-charge pumping at the FI/TI interface as a function of an applied voltage. By using realistic material parameters, we find that the effective damping for a FI with 10 nm thickness can be tuned by one order of magnitude under the voltage with 0.25 V. Also, we provide perspectives on the voltage-induced modulation of the magnon spin transport on proximity-coupled FIs.

Voltage or electric-field control of magnetic properties is fundamentally and technologically crucial for energetically efficient spintronic technologies,^{1,2} such as magnetic random-access memories (MRAMs),³ spin transistors,^{4,5} and spin-wave-based logic gates.⁶ In these technologies, voltage-control of magnetic anisotropy (VCMA) in thin ferromagnets^{7–9} promises energy-efficient reversal of magnetization by a pulsed voltage^{10–12} and manipulation of propagating spin waves with lower power consumption.¹³ The control of magnetic damping is also highly desirable to increase the performance of spintronic devices. For instance, low magnetic damping allows small critical current densities for magnetization switching and spin-wave excitation by current-induced spin-transfer¹⁴ and spin-orbit torques.^{15,16} On the other hand, a high magnetic damping can be beneficial in reducing the data writing time in MRAM devices. For magnonic devices, magnetic damping is a key factor because it governs the lifetime of spin waves or magnons as information carriers.¹⁷ Even if the magnetic damping is a vital material parameter that governs magnetization dynamics in several spintronic devices, its voltage-control is not fully explored except for a few experiments with ferro- and ferrimagnets.^{18–22}

The main origin of magnetic dissipation is the spin-orbit interaction (SOI), which creates relaxation paths of the spin-angular momentum into conduction electrons and the lattice. Hence, potential candidates to achieve the voltage-control of magnetic damping are magnetic materials and/or strong SOI systems. Three-dimensional topological insulators (3D TIs), such as Bi₂Se₃, are characterized by band inversion due to a strong SOI^{23,24} and possess an ideally insulating bulk and spin-momentum locked metallic surface states. Recently, Bi_{2–x}Sb_xTe_{3–y}Se_y (BSTS)²⁵ and Sn-doped Bi_{2–x}Sb_xTe₂S²⁶ have been reported to be ideal 3D TIs with two-dimensional (2D) Dirac electrons on the surface and a highly insulating bulk. For spintronics, the interface between a ferromagnet and a TI can enhance the magnitude of both spin and charge currents.^{27,28} Some experiments reported^{29–32} the spin-charge

conversion at room temperature^{33,34} in a bilayer of TI/ferro- and ferrimagnetic-insulator (FI) such as Y₃Fe₅O₁₂ (YIG) with very low Gilbert damping constant (α). An essential feature of the FI/TI bilayer is that the TI bulk behaves as a semiconductor, enabling the control of the surface carrier density by a voltage.³⁵ Also, magnetically doped TI exhibit VCMA.^{12,36} Hence, TIs are a promising candidate to achieve the voltage-control of magnetic damping.

In this work, we theoretically demonstrate the voltage-control of magnetic damping in FI/TI bilayers. We formulate an effective dissipation torque induced by spin-charge pumping at the FI/TI interface as a function of a gate voltage V_G . Our main result is that the voltage changes the effective damping by one order of magnitude for a FI with a perpendicular magnetization configuration and 10 nm thickness. Also, we provide perspectives on the modification of magnon scattering time in a FI-based magnonic device.

To study the effective damping torque, we consider 2D massless Dirac electrons on the TI surface with the magnetic proximity effect,^{29–32} i.e., coupled to the magnetization of an adjacent FI. The exchange interaction between the surface electrons and the FI magnetization is modeled by a constant spin splitting along the magnetization direction with unit vector $\mathbf{m} = \mathbf{M}/M_s$ (in which \mathbf{M} is the magnetization vector with the saturation magnetization M_s).³⁷ Then, the following 2D Dirac Hamiltonian provides a simple model for the FI/TI interface state³⁸:

$$\hat{H} = v_F \boldsymbol{\sigma} \cdot (\hat{\mathbf{p}} \times \hat{\mathbf{z}}) + \Delta \boldsymbol{\sigma} \cdot \mathbf{m}, \quad (1)$$

where \hbar is the reduced Planck constant, v_F is the Fermi velocity of the Dirac electrons at zero applied voltage, $\hat{\mathbf{p}} = -i\hbar\nabla$ is the momentum operator, $\{\hat{\mathbf{x}}, \hat{\mathbf{y}}, \hat{\mathbf{z}}\}$ are the unit vectors along the respective Cartesian axes, $\boldsymbol{\sigma} = (\sigma_x, \sigma_y, \sigma_z)$ is the vector of Pauli matrices for the spin, and Δ is the exchange interaction constant. For simplicity, we ignore here the particle–hole asymmetry and the hexagonal warping effect in the surface bands. Also, Δ and v_F are assumed to be temperature indepen-

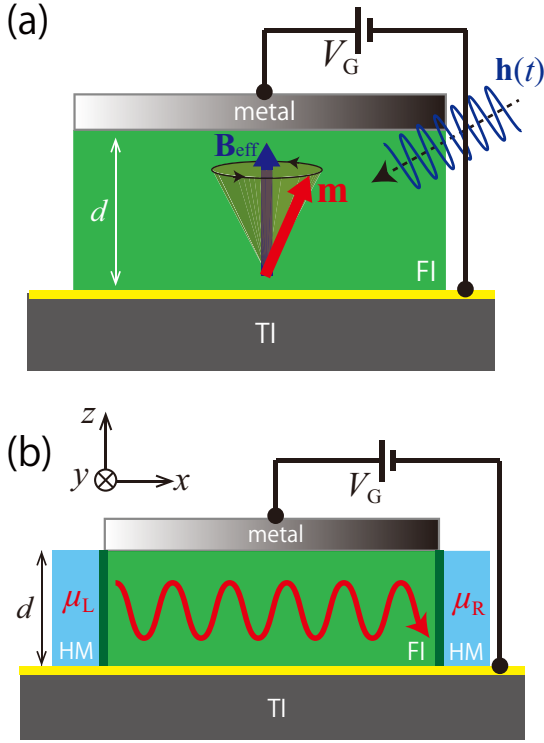


FIG. 1. (a) Schematic geometry (side view) of a capacitor-like device comprising a ferromagnetic insulator (FI) film (with thickness d) sandwiched by a TI and a normal metal as a top electric gate with V_G . The yellow line corresponds to the TI surface state. The red arrow denotes the precessional magnetization directions in the FMR driven by static (\mathbf{B}_{eff}) and oscillating ($\mathbf{h}(t)$) magnetic fields. (b) Schematic geometry of a transistor-like device comprising a FI film sandwiched by a TI and a normal metal. The red wave arrow represents a magnon current driven by the difference in spin accumulation ($\mu_L - \mu_R$) in the attached left and right heavy metal (HM) leads.

dent.⁴⁰ Note that we operate in the weak magnetic coupling limit, and therefore self-consistent treatment for the induced gap (Δ)³⁹ is not necessary.

Let us begin by calculating the dissipation torque induced by the spin-charge pumping^{28,41–43} of a dynamic magnetization in FI/TI bilayers. A precessing magnetization, driven by ferromagnetic resonance (FMR), as shown in Fig. 1, can be regarded as an effective vector potential $\mathbf{A}_{\text{eff}}(t) = \Delta/(ev_F)\hat{\mathbf{z}} \times \mathbf{m}(t)$ with the electron charge $-e$ ($e > 0$), which drives a charge current via an effective electric field $\mathbf{E}_{\text{eff}} = -\partial_t \mathbf{A}_{\text{eff}}$ (see the supplementary material), i.e.,

$$\mathbf{J}_P = \frac{\Delta}{ev_F} \left(\sigma_{\text{AH}} \frac{\partial \mathbf{m}}{\partial t} - \sigma_L \hat{\mathbf{z}} \times \frac{\partial \mathbf{m}}{\partial t} \right), \quad (2)$$

where σ_L and σ_{AH} are longitudinal and transverse (anomalous-Hall) conductivities, respectively, and depend on the z -component of the magnetization (m_z)³⁸. From the Hamiltonian (1), the velocity operator $\hat{\mathbf{v}} = \partial \hat{H} / \partial \hat{\mathbf{p}} = v_F \hat{\mathbf{z}} \times \boldsymbol{\sigma}$ depends linearly on $\boldsymbol{\sigma}$. Therefore, the nonequilibrium spin polarization $\boldsymbol{\mu}_P$ (in units of m^{-2}) is a linear function of the charge current \mathbf{J}_P on the TI surface, i.e., $\boldsymbol{\mu}_P = \hat{\mathbf{z}} \times \mathbf{J}_P / (ev_F)$.

This nonequilibrium spin polarization $\boldsymbol{\mu}_P$ exerts a dissipation torque on the magnetization, $\mathbf{T}_{\text{SP}} = -\gamma \Delta / (M_s d) \boldsymbol{\mu}_P \times \mathbf{m}$, namely

$$\mathbf{T}_{\text{SP}} = (-\alpha_{\text{AH}} m_z + \alpha_L \mathbf{m} \times) \left(\frac{\partial \mathbf{m}}{\partial t} - \frac{\partial m_z}{\partial t} \hat{\mathbf{z}} \right), \quad (3)$$

with

$$\alpha_{L(\text{AH})} = \frac{\gamma \Delta^2}{e^2 v_F^2 M_s d} \sigma_{L(\text{AH})}, \quad (4)$$

where γ is the gyromagnetic ratio and d is the thickness of the FI layer. Equation (3) is equivalent to the charge-pumping-induced damping-like torque that *Ndiaye et al.* derived using the Onsager reciprocity relation for a current-induced spin-orbit torque.⁴³ The first term in Eq. (3) originates from the magnetoelectric coupling (the Chern–Simons term)^{37,44} and renormalizes the gyromagnetic ratio. By using parameters listed in TABLE I, $\Delta = 40$ meV, and $d = 10$ nm, $\alpha_{\text{AH}} \approx 10^{-4}$ is estimated even by using σ_{AH} at 0 K as the upper value.³⁸ Thus, we disregard the renormalization of the gyromagnetic ratio. In contrast, the second term in Eq. (3) stems from the Rashba–Edelstein effect due to the spin-momentum locking on the TI surface⁴¹ and contributes to magnetic damping. Since we are interested in voltage-control of magnetic damping, we hereafter focus on α_L in this study.

According to Eq. (4), the electric field effect on the conductivity σ_L can be used to control the magnetic dissipation. Namely, the voltage-induced change of the interfacial density of states in σ_L renders the TI a more or less efficient spin sink. The damping enhancement α_L depends on the chemical potential μ , measured from the original band-touching (Dirac) point. At room temperature, or below it, the thermal energy is much smaller than the Fermi one, $k_B T \ll E_F$, with T the temperature and k_B the Boltzmann constant. Then, we can use the following Sommerfeld expansion of the chemical potential μ

$$\mu(T) \approx E_F \left[1 - \frac{\pi^2}{6} \left(\frac{k_B T}{E_F} \right)^2 \right] \quad (5)$$

with the voltage-dependent Fermi energy,¹² $E_F = \mu(0)$, given by

$$E_F(V_G) = \hbar v_F \sqrt{4\pi \left(n_{\text{int}} + \frac{\Delta^2}{4\pi (\hbar v_F)^2} + \frac{\epsilon}{ed} V_G \right)}, \quad (6)$$

where ϵ is the permittivity of a FI and $n_{\text{int}} = (E_F^2(0) - \Delta^2) / (4\pi \hbar^2 v_F^2)$ is the intrinsic carrier density, i.e., at $V_G = 0$. Note that we can define a voltage-dependent surface electron density $n_V(V_G) \equiv n_{\text{int}} + \epsilon V_G / (ed)$ that shows the underlying mechanism behind the voltage-control of interfacial phenomena in insulating bilayers with surface carriers, which goes beyond topological materials. Namely, a voltage increases or decreases the effective electron density and therefore enhances or weakens all effects that depend on this density, including isotropic⁴⁵ and anisotropic⁴⁶ exchange interactions, emergence of magnetization in metals,⁴⁷ perpendicular magnetic anisotropy,^{3,9} and spin-orbit torques.¹² The

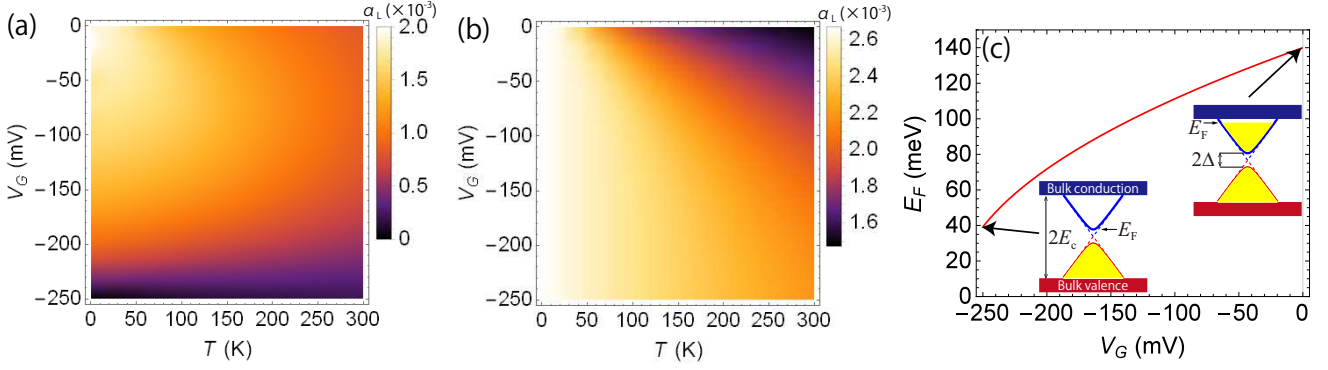


FIG. 2. Effective damping enhancement α_L of a TI/FI bilayer as functions of V_G and T for $E_F(V_G = 0) = 140$ meV: (a) $m_z = 1$, (b) $m_z = 0$. (c) Voltage modulation of E_F in a TI. Insets represent schematic of massless (dashed line) and massive (solid line) surface state dispersions in the bulk band gap. In these graphs, we use parameters listed in Table I, $\Delta = 40$ meV, and $d = 10$ nm for a FI thickness. The details of the calculations are given in the text.

voltage-generated change in the surface density is equivalent to an interfacial Fermi energy shift. In this work, we predict that the spin-charge pumping efficiency is also modulated, an effect that may also appear in usual FI|*normal metal* bilayers since the spin-mixing conductance depends on the electronic density.⁴⁸

We investigate the effect of electric-gate on the effective damping α_L so that we assume hereafter that the low-energy Dirac Hamiltonian (1) is an accurate description for a momentum cut $k_c = \sqrt{E_c^2 - \Delta^2}/(\hbar v_F)$, in which $2E_c$ is the bulk bandgap of TIs⁵⁰ (see Fig. 2 (c)). Sufficiently far from the Dirac point ($\hbar\tau/E_F \ll 1$, τ is the transport relaxation time), the electron scattering can be treated by the first Born approximation.⁵¹ With this, the longitudinal conductivity reads⁵²

$$\sigma_L = \frac{e^2}{2\hbar} \int_{-E_c}^{E_c} dE_k \frac{E_k \tau(E_k, T)}{\hbar} \frac{E_k^2 - \Delta^2 m_z^2}{E_k^2 + 3\Delta^2 m_z^2} \left(-\frac{\partial f_{\text{FD}}}{\partial E_k} \right), \quad (7)$$

where $f_{\text{FD}} = [\exp\{(E_k - \mu)/(k_B T)\} + 1]^{-1}$ is the Fermi-Dirac distribution, the energy E_k is the eigenvalue of Eq. (1), and $\tau(E_k, T)$ is the transport relaxation time of massless Dirac electrons within the Born approximation for impurity and phonon scatterings. By applying the Matthiessen rule,

$$\frac{1}{\tau(E_k, T)} = E_k (a + b k_B T), \quad (8)$$

where $a = nV_0^2/(4\hbar^3 v_F^2)$ (in units of $\text{eV}^{-1}\text{s}^{-1}$) parameterize contribution of the impurity scattering,^{53,54} n is the impurity concentration, and V_0 is the scattering potential. Also, contribution to the transport relaxation time from the phonon scattering^{53,54} can be approximated by $b = D_0^2/(4\hbar^3 v_F^2 \rho t_s v_L^2)$ (in units of $\text{eV}^{-2}\text{s}^{-1}$), where ρ is the mass density of the quintuple layer (QL) in the TI crystal structure, t_s is the thickness of one atomic layer in 1 QL of TIs, v_L is the longitudinal phonon velocity, and D_0 is the deformation potential constant.

Figures 2 (a) and (b) show the V_G and T dependence of the effective damping enhancement α_L for out-of-plane ($m_z = 1$) and in-plane ($m_z = 0$) magnetization configurations, respectively. Also, Fig. 2 (c) illustrates the voltage modulation of

TABLE I. Material parameters for the TI/FI bilayer.

	Symbol	Value	Unit
^a BSTS Fermi velocity	v_F	4.0×10^5	ms^{-1}
^a BSTS bulk band gap	$2E_c$	300	meV
^b YIG gyromagnetic ratio	γ	1.76×10^{11}	$\text{T}^{-1}\text{s}^{-1}$
^b YIG Gilbert damping constant	α	6.7×10^{-5}	
^b YIG saturation magnetization	M_s	1.56×10^5	Am^{-1}
^c YIG relative permittivity	ϵ/ϵ_0	15	

^aReference 25, ^bReference 33, ^cReference 49.

E_F in TI. The bulk damping constant can be influenced by material and device parameters, such as SOI and magnetic anisotropies³⁴. However, we predict the voltage-modulation of the *damping enhancement* by spin-charge pumping. Therefore, our results are independent of the intrinsic dissipation mechanisms. At the FI/TI interface, orbital hybridization between TI and the 3d transition metal in FI, such as YIG, deforms the TI surface states, which might shift the Dirac point to the lower energy and lift up E_F ,⁵⁵ so that we consider relatively high value $E_F(V_G = 0) = 140$ meV with the corresponding carrier density of the order of 10^{12} cm^{-2} . Also, Δ is used within the values reported experimentally in FI-attached TIs.^{56,57} For impurity parameters, we use $n = 10^{11} \text{ cm}^{-2}$ and $V_0 = 0.15 \text{ keV}\text{\AA}^2$ based on an analysis of the transport properties of a TI surface.⁵² We could not find estimates of the phonon scattering for BSTS in the literature so that we adopt those of non-substituted Bi_2Te_3 being $v_L = 2.9 \times 10^5 \text{ ms}^{-1}$, $D_0 = 35 \text{ eV}$, $t_s = 0.16 \text{ nm}$, and $\rho = 7.86 \times 10^3 \text{ kgm}^{-3}$ in Ref. 58. These scattering parameters describe a relatively clean interface with the sheet resistance $\sim 1 \text{ k}\Omega$, which is one order less than that of experiments. In Figs. 2 (a) and (b), α_L monotonically decreases with increasing T at a fixed V_G while it has peaks for changing V_G at a fixed $T > 0$ (see also the inset of Fig. 3). This feature reflects thermal excitation of surface carriers into the bulk states ($E_k > E_c$), reducing the spin-charge-pumping contribution. With the out-of-plane configura-

ration, α_L can be tuned by one order of magnitude under the voltage, while α_L changes by less than a factor two with the in-plane state, which suggests that the out-of-plane configuration is superior in controllability. The calculated T dependence of damping enhancement at $V_G = 0$ for the in-plane configuration agrees with a few experiments with the FI/TI bilayer.^{31,59} Note that at much lower than $E_F(V_G = -250 \text{ mV}) \approx 40 \text{ meV}$, our calculation with the in-plane configuration breaks down because of the finite level broadening due to the higher-order impurity scattering.⁶⁰ The V_G -dependent FMR is characterized by the Landau-Lifshitz-Gilbert theory in the supplementary material.

The electric manipulation of magnon spin transport is a relevant topic in spintronics. For example, in YIG with an injector and a detector Pt contact, changes of the magnon spin conductivity can be obtained by using a third electrode that changes the magnon density,^{61–63} potentially providing a functionality similar to the one a *field-effect transistors*. Damping compensation by current-driven torques^{64,65} in magnetic heterostructures also influences magnon transport. Here, we provide a perspective on the electric-field-induced modulation of magnon scattering time, τ_m . Magnons can be injected and detected by their interconversion with charge currents in adjacent heavy metals (HMs) through the direct and inverse spin-Hall effects.³³ Similar to charge transport induced by an electrochemical potential gradient, a magnon spin current can be driven by the gradient of a magnon chemical potential injected by an external source.^{66,67} Magnon transport through a FI can be controlled by the gate voltage that modulates the effective damping in Eq. (4).

So far, the magnon spin transport in the FI/TI bilayer lacks microscopic theory with few exceptions.^{68,69} However, from the bulk of magnon spin transport,⁶⁶ the control of τ_m results in the modification of all transport properties, including the magnon spin conductivity. In the presence of a TI contact, interfacial magnons are scattered by conducting Dirac electrons on the TI surface.⁷⁰ Considering a very thin ferromagnet that can be modeled by a 2D magnet. The inset of Fig. 3 shows that the damping enhancement is at least one order of magnitude larger than the bulk one of YIG.^{33,34} Accordingly, let us assume that interfacial magnons are absorbed by transferring their energy and angular momentum to Dirac electrons at a rate $1/\tau_m \propto \alpha_L$.⁶⁶ While there is no known microscopic expression for the magnon spin conductivity in the present system, bulk magnon transport obeys the relationship $\sigma_m \propto \tau_m$,^{61,62} where σ_m is the magnon spin conductivity. In our case, the scattering time τ_m is dominated by the magnon-relaxation process into the FI/TI interface. To estimate an effect of electric-gate on the magnon spin transport, we define the modulation efficiency

$$\eta_m = \frac{\tau_m(V_G) - \tau_m(V_{\max})}{\tau_m(V_{\max})} = \frac{\alpha_L(V_{\max})}{\alpha_L(V_G)} - 1, \quad (9)$$

where V_{\max} ($\approx -68 \text{ mV}$ for Fig. 3) gives the maximum value of α_L (and therefore the minimum value of τ_m). In principle, τ_m depends on V_G through not only α_L but also via magnon dispersion relation, $\hbar\omega_q$,⁶⁶ including a V_G -dependent magnetic anisotropy. However, this V_G -dependence is quite small

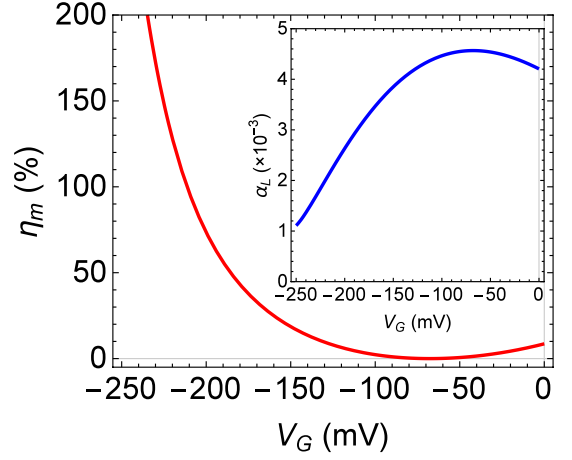


FIG. 3. Modulation efficiency (η_m) as a function of the gate voltage. Inset shows the corresponding behavior of the effective damping enhancement α_L . In these graphs, we use parameters listed in Table I, $\Delta = 40 \text{ meV}$, and $d = 2 \text{ nm}$ for a FI thickness. We also set $E_F(V_G = 0) = 140 \text{ meV}$ and $T = 300 \text{ K}$.

even for a FI with 2 nm thickness (see the supplementary material), so that we disregard the influence of the magnon gap in the following calculation. Figure 3 shows V_G -dependence of the modulation efficiency at room temperature in which the strongly nonlinear behavior is interpreted as follows. Down to $V_G \approx -130 \text{ mV}$, α_L is affected by the thermal excitation of surface carriers, which makes a peak around $V_G \approx -70 \text{ mV}$. From -130 mV to -250 mV , the thermal excitation is suppressed, so that α_L monotonically decreases with $|V_G|$ due to the reduction of the Fermi surface. Hence, in this regime, one can effectively modulate the magnon spin transport by the voltage.

In summary, we have theoretically demonstrated the voltage-control of magnetic damping in ferro- ferrimagnetic insulator (FI)/topological insulator (TI) bilayers. Assuming a capacitor-like setup, we formulate an effective damping torque induced by spin-charge pumping at the FI/TI interface as a gate voltage function. The presence of a perpendicular electric field results in a shift of the Fermi level or, equivalently, a modified interfacial electron density, increasing or decreasing the efficiency of the pumping process. We studied the consequences of this damping enhancement using realistic material parameters for FI and TI. We found that the effective damping with the out-of-plane magnetization configuration can be modulated by one order of magnitude under the voltage with 0.25 V. The present results motivate an application: the magnon scattering time can be tuned by a gate voltage, potentially allowing for a magnon transistor type of application. A complete quantitative description of the latter requires a microscopic theory of magnon spin transport in FI/TI bilayers, which might remain an unexplored issue. The voltage-control of magnetic damping paves the way for low-power spintronic and magnonic technologies beyond the current-based control.

See the supplementary material for the calculation of the

spin-charge pumping in FI/TI bilayers, the characterization of the FMR under several values of the applied voltage, the influence of V_G -dependence of the anisotropy in the magnon dispersion.

We thank Camilo Ulloa and Nicolas Vidal-Silva for fruitful discussions. This work was supported by Grants-in-Aid for Scientific Research (Grant No. 20K15163 and No. 20H02196) from the JSPS and Postdoctorado FONDECYT 2019 Folio 3190030.

DATA AVAILABILITY

The data that support the findings of this study are available from the corresponding author upon reasonable request.

- ¹H. Ohno, D. Chiba, F. Matsukura, T. Omiya, E. Abe, T. Dietl, Y. Ohno, and K. Ohtani, "Electric-field control of ferromagnetism," *Nature* **408**, 944 (2000).
- ²C. Song, B. Cui, F. Li, X. Zhou, and F. Pan, "Recent progress in voltage control of magnetism: Materials, mechanisms, and performance," *Prog. Mater. Sci.* **87**, 33 (2017).
- ³T. Nozaki, T. Yamamoto, S. Miwa, M. Tsujikawa, M. Shirai, S. Yuasa, and Y. Suzuki, "Recent Progress in the Voltage-Controlled Magnetic Anisotropy Effect and the Challenges Faced in Developing Voltage-Torque MRAM," *Micromachines* **10**, 327 (2019).
- ⁴I. Žutić, J. Fabian, and S. Das Sarma, "Spintronics: Fundamentals and applications," *Rev. Mod. Phys.* **76**, 323 (2004).
- ⁵K. Takiguchi, L. D. Anh, T. Chiba, T. Koyama, D. Chiba, and M. Tanaka, "Giant gate-controlled proximity magnetoresistance in semiconductor-based ferromagnetic-non-magnetic bilayers," *Nat. Phys.* **15**, 1134 (2019).
- ⁶B. Rana and Y. Otani, "Towards magnonic devices based on voltage-controlled magnetic anisotropy," *Commun. Phys.* **2**, 90 (2019).
- ⁷M. Weisheit, S. F'ahler, A. Marty, Y. Souche *et al.*, "Electric field-induced modification of magnetism in thin-film ferromagnets," *Science* **315**, 349 (2007).
- ⁸C.-G. Duan, J. P. Velev, R. F. Sabirianov, Z. Zhu, J. Chu, S. S. Jaswal, and E. Y. Tsymlal, "Surface magnetoelectric effect in ferromagnetic metal films," *Phys. Rev. Lett.* **101**, 137201 (2008).
- ⁹T. Maruyama, Y. Shiota, T. Nozaki, K. Ohta *et al.*, "Large voltage-induced magnetic anisotropy change in a few atomic layers of iron," *Nat. Nanotech.* **4**, 158 (2009).
- ¹⁰Y. Shiota, T. Nozaki, F. Bonell, S. Murakami, T. Shinjo, and Y. Suzuki, "Induction of coherent magnetization switching in a few atomic layers of FeCo using voltage pulses," *Nat. Mater.* **11**, 39 (2012).
- ¹¹A. O. Leon, A. B. Cahaya, and G. E. W. Bauer, "Voltage Control of Rare-Earth Magnetic Moments at the Magnetic-Insulator-Metal Interface," *Phys. Rev. Lett.* **120**, 027201 (2018).
- ¹²T. Chiba and T. Komine, "Voltage-Driven Magnetization Switching via Dirac Magnetic Anisotropy and Spin-Orbit Torque in Topological-Insulator-Based Magnetic Heterostructures," *Phys. Rev. Appl.* **14**, 034031 (2020).
- ¹³B. Rana and Y. Otani, "Voltage-Controlled Reconfigurable Spin-Wave Nanochannels and Logic Devices," *Phys. Rev. Appl.* **9**, 224412 (2019).
- ¹⁴D. C. Ralph and M. D. Stiles, "Spin transfer torques," *J. Magn. Mag. Mater.* **320**, 1190 (2008).
- ¹⁵A. Manchon, J. Železný, I. M. Miron, T. Jungwirth, J. Sinova, A. Thiaville, K. Garello, and P. Gambardella, "Current-induced spin-orbit torques in ferromagnetic and antiferromagnetic systems," *Rev. Mod. Phys.* **91**, 035004 (2019).
- ¹⁶A. Hamadeh, O. d'Allivy Kelly, C. Hahn, H. Meley, R. Bernard, A. H. Molpeceres, V. V. Naletov, M. Viret, A. Anane, V. Cros, S. O. Demokritov, J. L. Prieto, M. Muñoz, G. de Loubens, and O. Klein, "Full Control of the Spin-Wave Damping in a Magnetic Insulator Using Spin-Orbit Torque," *Phys. Rev. Lett.* **113**, 197203 (2014).
- ¹⁷A. V. Chumak, V. I. Vasuychka, A. A. Serga, and B. Hillebrands, "Magnon spintronics," *Nat. Phys.* **11**, 453 (2015).
- ¹⁸A. Okada, S. Kanai, M. Yamanouchi, S. Ikeda, F. Matsukura, and H. Ohno, "Electric-field effects on magnetic anisotropy and damping constant in Ta/CoFeB/MgO investigated by ferromagnetic resonance," *Appl. Phys. Lett.* **105**, 052415 (2014).
- ¹⁹L. Chen, F. Matsukura, and H. Ohno, "Electric-field Modulation of Damping Constant in a Ferromagnetic Semiconductor (Ga,Mn)As," *Phys. Rev. Lett.* **115**, 057204 (2015).
- ²⁰B. Rana, C. Ashu Akosa, K. Miura, H. Takahashi, G. Tatara, and Y. Otani, "Nonlinear Control of Damping Constant by Electric Field in Ultrathin Ferromagnetic Films," *Phys. Rev. Appl.* **14**, 014037 (2020).
- ²¹S.-J. Xu, X. Fan, S.-M. Zhou, X. Qiu, and Z. Shi, "Gate voltage tuning of spin current in Pt/yttrium iron garnet heterostructure," *J. Phys. D: Appl. Phys.* **52**, 175304 (2019).
- ²²L. Wang, Z. Lu, J. Xue, P. Shi, Y. Tian, Y. Chen, S. Yan, L. Bai, and M. Harder, "Electrical Control of Spin-Mixing Conductance in a $Y_3Fe_5O_{12}$ /Platinum Bilayer," *Phys. Rev. Appl.* **11**, 044060 (2019).
- ²³M. Z. Hasan and C. L. Kane, "Rev. Colloquium: Topological insulators," *Mod. Phys.* **82**, 3045 (2010).
- ²⁴X.-L. Qi and S.-C. Zhang, "Topological insulators and superconductors," *Rev. Mod. Phys.* **83**, 1057 (2011).
- ²⁵Y. Ando, "Topological insulator materials," *J. Phys. Soc. Jpn.* **82**, 102001 (2013).
- ²⁶S. K. Kushwaha, I. Pletikosić, T. Liang, A. Gyenis *et al.*, "Sn-doped $Bi_{1.1}Sb_{0.9}Te_2S$ bulk crystal topological insulator with excellent properties," *Nat. Commun.* **7**, 11456 (2016).
- ²⁷A. R. Mellnik, J. S. Lee, A. Richardella, J. L. Grab, P. J. Mintun, M. H. Fischer, A. Vaezi, A. Manchon, E.-A. Kim, N. Samarth, and D. C. Ralph, "Spin-transfer torque generated by a topological insulator," *Nature* **511**, 449 (2014).
- ²⁸Y. Shiomi, K. Nomura, Y. Kajiwara, K. Eto, M. Novak, K. Segawa, Y. Ando, and E. Saitoh, "Spin-Electricity Conversion Induced by Spin Injection into Topological Insulators," *Phys. Rev. Lett.* **113**, 196601 (2014).
- ²⁹Z. Jiang, C.-Z. Chang, M. R. Masir, C. Tang, Y. Xu, J. S. Moodera, A. H. MacDonald, and J. Shi, "Enhanced spin Seebeck effect signal due to spin-momentum locked topological surface states," *Nat. Commun.* **7**, 11458 (2016).
- ³⁰H. Wang, J. Kally, J. S. Lee, T. Liu, H. Chang, D. Reifsnnyder, H. K. A. Mkhoyan, M. Wu, A. Richardella, and N. Samarth, "Surface-State-Dominated Spin-Charge Current Conversion in Topological-Insulator-Ferromagnetic-Insulator Heterostructures," *Phys. Rev. Lett.* **117**, 076601 (2016).
- ³¹C. Tang, Q. Song, C.-Z. Chang, Y. Xu, Y. Ohnuma, M. Matsuo, Y. Liu, W. Yuan, Y. Yao, J. S. Moodera, S. Maekawa, W. Han, and J. Shi, "Dirac surface state-modulated spin dynamics in a ferrimagnetic insulator at room temperature," *Sci. Adv.* **4**, eaas8660 (2018).
- ³²Y. T. Fanchiang, K. H. M. Chen, C. C. Tseng, C. C. Chen, C. K. Cheng, S. R. Yang, C. N. Wu, S. F. Lee, M. Hong, and J. Kwo, "Strongly exchange-coupled and surface-state-modulated magnetization dynamics in Bi_2Se_3 /yttrium iron garnet heterostructures," *Nat. Commun.* **9**, 223 (2018).
- ³³Y. Kajiwara, K. Harii, S. Takahashi, J. Ohe, K. Uchida, M. Mizuguchi, H. Umezawa, H. Kawai, K. Ando, K. Takanashi, S. Maekawa, and E. Saitoh, "Transmission of electrical signals by spin-wave interconversion in a magnetic insulator," *Nature* **464**, 262 (2010).
- ³⁴J. Ding, C. Liu, Y. Zhang, U. Erugu, Z. Quan, R. Yu, E. McCollum, S. Mo, S. Yang, H. Ding, X. Xu, J. Tang, X. Yang, and M. Wu, "Nanometer-Thick Yttrium Iron Garnet Films with Perpendicular Anisotropy and Low Damping," *Phys. Rev. Appl.* **14**, 014017 (2020).
- ³⁵H. Wang, J. Kally, C. Sahin, T. Liu, W. Yanez, E. J. Kamp, A. Richardella, M. Wu, M. E. Flatté, and N. Samarth, "Fermi level dependent spin pumping from a magnetic insulator into a topological insulator," *Phys. Rev. Res.* **1**, 012014(R) (2019).
- ³⁶Y. Fan, X. Kou, P. Upadhyaya, Q. Shao, L. Pan, M. Lang, X. Che, J. Tang, M. Montazeri, K. Murata, L.-T. Chang, M. Akyol, G. Yu, T. Nie, K. L. Wong, J. Liu, Y. Wang, Y. Tserkovnyak, and K. L. Wang, "Electric-field control of spin-orbit torque in a magnetically doped topological insulator," *Nat. Nanotechnol.* **11**, 352 (2016).
- ³⁷K. Nomura and N. Nagaosa, "Electric charging of magnetic textures on the surface of a topological insulator," *Phys. Rev. B* **82**, 161401(R) (2010).
- ³⁸T. Chiba, S. Takahashi, and G. E. W. Bauer, "Magnetic-proximity-induced magnetoresistance on topological insulators," *Phys. Rev. B* **95**, 094428 (2017).

- (2017).
- ³⁹D. K. Efimkin and V. Galitski, "Self-consistent theory of ferromagnetism on the surface of a topological insulator," *Phys. Rev. B* **89**, 115431 (2014).
- ⁴⁰Z.-H. Pan, E. Vescovo, A. V. Fedorov, G. D. Gu, and T. Valla, "Persistent coherence and spin polarization of topological surface states on topological insulators," *Phys. Rev. B* **88**, 041101(R) (2013).
- ⁴¹T. Yokoyama, J. Zang, and N. Nagaosa, "Theoretical study of the dynamics of magnetization on the topological surface," *Phys. Rev. B* **81**, 241410(R) (2010).
- ⁴²A. Sakai and H. Kohno, "Spin torques and charge transport on the surface of topological insulator," *Phys. Rev. B* **89**, 165307 (2014).
- ⁴³P. B- Ndiaye, C. A. Akosa, M. H. Fischer, A. Vaezi, E-A. Kim, and A. Manchon, "Dirac spin-orbit torques and charge pumping at the surface of topological insulators," *Phys. Rev. B* **96**, 014408 (2017).
- ⁴⁴I. Garate and M. Franz, "Inverse Spin-Galvanic Effect in the Interface between a Topological Insulator and a Ferromagnet," *Phys. Rev. Lett.* **104**, 146802 (2010).
- ⁴⁵A. O. Leon, J. d'A Castro, J. C. Retamal, A. B. Cahaya, and D. Altbir, "Manipulation of the RKKY exchange by voltages," *Phys. Rev. B* **100**, 014403 (2019).
- ⁴⁶K. Nawaoka, S. Miwa, Y. Shiota, N. Mizuochi, and Y. Suzuki, "Voltage induction of interfacial Dzyaloshinskii-Moriya interaction in Au/Fe/MgO artificial multilayer," *Appl. Phys. Express* **8**, 063004 (2015).
- ⁴⁷S. Miwa, M. Suzuki, M. Tsujikawa, K. Matsuda *et al.*, "Voltage controlled interfacial magnetism through platinum orbits," *Nat. Comm.* **8**, 15848 (2017).
- ⁴⁸A. B. Cahaya, A. O. Leon, and G. E. W. Bauer, "Crystal field effects on spin pumping," *Phys. Rev. B* **96**, 144434 (2017).
- ⁴⁹K. Sadhana, R. S. Shinde, and S. R. Murthy, "Synthesis of nanocrystalline yig using microwave-hydrothermal method," *International Journal of Modern Physics B* **23**, 3637-3642 (2009), publisher: World Scientific Publishing Co.
- ⁵⁰Y. Tserkovnyak, D. A. Pesin, and D. Loss, "Spin and orbital magnetic response on the surface of a topological insulator," *Phys. Rev. B* **91**, 041121(R) (2015).
- ⁵¹S. Adam, P. W. Brouwer, and S. Das Sarma, "Crossover from quantum to Boltzmann transport in graphene," *Phys. Rev. B* **79**, 201404(R) (2009).
- ⁵²T. Chiba and S. Takahashi, "Transport properties on an ionically disordered surface of topological insulators: Toward high-performance thermoelectrics," *J. Appl. Phys.* **126**, 245704 (2019).
- ⁵³Y. V. Ivanov, A. T. Burkov, and D. A. P-Severin, "Thermoelectric properties of topological insulators," *Phys. Status Solidi B* **255** 1800020 (2018).
- ⁵⁴S. Giraud, A. Kundu, and R. Egger, "Electron-phonon scattering in topological insulator thin films," *Phys. Rev. B* **85**, 035441 (2012).
- ⁵⁵J. M. Marmolejo-Tejada, K. Dolui, P. Lazić, P.-H. Chang, S. Smidstrup, D. Stradi, K. Stokbro, and B. K. Nikolić, "Proximity Band Structure and Spin Textures on Both Sides of Topological-Insulator/Ferromagnetic-Metal Interface and Their Charge Transport Probes," *Nano Lett.* **17**, 5626 (2017).
- ⁵⁶T. Hirahara, S. V. Eremeev, T. Shirasawa, Y. Okuyama, T. Kubo, R. Nakanishi, R. Akiyama, A. Takayama, T. Hajiri, S. Ideta *et al.*, "Large-gap magnetic topological heterostructure formed by subsurface incorporation of a ferromagnetic layer," *Nano. Lett.* **17**, 3493 (2017).
- ⁵⁷M. Mogi, T. Nakajima, V. Ukleev, A. Tsukazaki, R. Yoshimi, M. Kawamura, K. S. Takahashi, T. Hanashima, K. Kakurai, T. Arima, M. Kawasaki, and Y. Tokura, "Large Anomalous Hall Effect in Topological Insulators with Proximitized Ferromagnetic Insulators," *Phys. Rev. Lett.* **123**, 016804 (2019).
- ⁵⁸B.-L. Huang and M. Kaviani, "Ab initio and molecular dynamics predictions for electron and phonon transport in bismuth telluride," *Phys. Rev. B* **77**, 125209 (2008).
- ⁵⁹T. Liu, J. Kally, T. Pillsbury, C. Liu, H. Chang, J. Ding, Y. Cheng, M. Hilde, R. E.-Herbert, A. Richardella, N. Samarth, and M. Wu, "Changes of Magnetism in a Magnetic Insulator due to Proximity to a Topological Insulator," *Phys. Rev. Lett.* **125**, 017204 (2020).
- ⁶⁰N. H. Shon and T. Ando, "Quantum Transport in Two-Dimensional Graphite System," *J. Phys. Soc. Jpn.* **67**, 2421 (1998).
- ⁶¹L. J. Cornelissen, J. Liu, B. J. van Wees, and R. A. Duine, "Spin-Current-Controlled Modulation of the Magnon Spin Conductance in a Three-Terminal Magnon Transistor," *Phys. Rev. Lett.* **120**, 097702 (2018).
- ⁶²J. Liu, X.-Y. Wei, B. J. van Wees, G. E. W. Bauer, and J. Ben Youssef, "Electrically induced strong modulation of magnons transport in ultrathin magnetic insulator films," arXiv:2011.07800v1.
- ⁶³O. Alves Santos, F. Feringa, K.S. Das, J. Ben Youssef, and B.J. van Wees, "Efficient Modulation of Magnon Conductivity in $Y_3Fe_5O_{12}$ Using Anomalous Spin Hall Effect of a Permalloy Gate Electrode," *Phys. Rev. Applied* **15**, 014038 (2021).
- ⁶⁴V. E. Demidov, S. Urazhdin, A. B. Rinkevich, G. Reiss, and S. O. Demokritov, "Spin Hall controlled magnonic waveguides," *Appl. Phys. Lett.* **104**, 152402 (2014).
- ⁶⁵T. Wimmer, M. Althammer, L. Liensberger, N. Vlietstra, S. Geprägs, M. Weiler, R. Gross, and H. Huebl, "Spin Transport in a Magnetic Insulator with Zero Effective Damping," *Phys. Rev. Lett.* **123**, 257201 (2019).
- ⁶⁶L. J. Cornelissen, K. J. H. Peters, G. E. W. Bauer, R. A. Duine, and B. J. van Wees, "Magnon spin transport driven by the magnon chemical potential in a magnetic insulator", *Phys. Rev. B* **94**, 014412 (2016).
- ⁶⁷V. Basso, E. Ferraro, and M. Piazza, "Thermodynamic transport theory of spin waves in ferromagnetic insulators," *Phys. Rev. B* **94**, 144422 (2016).
- ⁶⁸N. Okuma and K. Nomura, "Microscopic derivation of magnon spin current in a topological insulator/ferromagnet heterostructure," *Phys. Rev. B* **95**, 115403 (2017).
- ⁶⁹Y. Imai, and H. Kohno, "Theory of Cross-correlated Electron-Magnon Transport Phenomena: Case of Magnetic Topological Insulator," *J. Phys. Soc. Jpn.* **87**, 073709 (2018).
- ⁷⁰K. Yasuda, A. Tsukazaki, R. Yoshimi, K. S. Takahashi, M. Kawasaki, and Y. Tokura, "Large Unidirectional Magnetoresistance in a Magnetic Topological Insulator," *Phys. Rev. Lett.* **117**, 127202 (2016).